Heliyon 10 (2024) e38641

Contents lists available at ScienceDirect

Heliyon

journal homepage: www.cell.com/heliyon

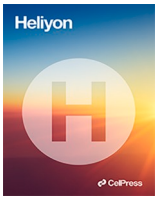

Research article

Comprehensive analysis of multiple regulated cell death risk signatures in lung adenocarcinoma

Shan Gao [1], Jiaqi Huang [1], Rui Zhao, Haiqi He, Jia Zhang, Xiaopeng Wen [*]

Department of Thoracic Surgery, First Affiliated Hospital of Xi'an Jiaotong University, Xi'an, 710061, China

A R T I C L E I N F O

Keywords:
Lung cancer
regulated cell death
Prognosis
Immunotherapy
Bioinformatic analysis

A B S T R A C T

Background: Regulated cell death (RCD) has considerable impact on tumor progress and sensitivity of treatment. Lung adenocarcinoma (LUAD) show a high resistance for conventional radiotherapies and chemotherapies. Currently, regulation of cancer cell death has been emerging as a new promising therapeutic avenue for LUAD patients. However, the crosstalk in each pattern RCD is unclear.

Methods: We integrated collected the hub-genes of 12 RCD subroutines and compressively analyzed these hub-genes synergistic effect in LUAD. The characters of RCD genes expression and prognosis were developed in The Cancer Genome Atlas (TCGA)-LUAD data. We developed and validated an RCD risk model based on TCGA and GSE70294 data set, respectively. Functional annotation and tumor immunotherapy based on the risk model were also investigated.

Results: 28 RCD-related genes and two LUAD molecular cluster were identified. Survival analysis revealed that the prognosis in high-risk group was worser than those in low-risk group. Functional enrichment analysis indicated that the RCD risk model correlated with immune responses. Further analysis indicated that the high-risk group in RCD risk model exhibited an immunosuppressive microenvironment and a lowly immunotherapy responder ratio.

Conclusions: We present an RCD risk model which have a promising ability in predicting LUAD prognosis and immunotherapy response.

1. Introdution

Lung cancer, the second frequently occurring cancer and the leading cause of cancer death in 2020, is classified into small-cell lung cancer (15 % of total diagnoses) and non-small-cell lung cancer (85 % of total diagnoses), which is subdivided into squamous and non-squamous histology that dominated by adenocarcinomas [1,2]. Often, lung cancer is not diagnosed until advanced-stage, which partly determines its high mortality [3]. Fortunately, low-dose CT-based screening in asymptomatic individuals substantially reduced lung cancer mortality [4]. The treatment strategy in patients with lung cancer is guided by the disease subtype and stage [5,6]. With the advent of targeted therapy, including immunotherapy, substantial progress has achieved in the medical therapy of lung cancer during the last decade. And knowledge of the molecular characteristics of a tumor reflected by specific biomarkers becomes an essential component of the more targeted therapeutic approach [7].

Regulated cell death (RCD) refers to the autonomous and orderly death of cells controlled by genes in order to maintain the stability

* Corresponding author.
E-mail address: xiaopengwen@xjtufh.edu.cn (X. Wen).
[1] Gao Shan and Huang Jiaqi contributed equally to this paper as first author.

https://doi.org/10.1016/j.heliyon.2024.e38641
Received 24 May 2024; Received in revised form 22 September 2024; Accepted 26 September 2024
Available online 27 September 2024

of the internal environment. RCD encompasses orchestrate subroutines, including apoptosis, autophagy, necroptosis, pyroptosis, ferroptosis, parthanatos, entosis, NETosis and lysosome-dependent cell death (LCD) and so on. In the aspect of molecular mechanism, each of RCD patterns exhibited a considerable degree of interconnection [8,9]. Accumulating evidence has revealed that abnormal RCD subroutines are the key features of tumorigenesis [10]. Apoptosis, as a natural barrier that protects against cancer development, is responsible for the programmed culling of cells during normal eukaryotic development and maintenance of organismal homeostasis [11,12]. Apoptosis evasion and resistance are indisputable hallmarks of cancer, that induced tumorigenesis and drug resistance [13,14]. Pyroptosis is redefined as gasdermin-mediated programmed necrosis and is accompanied by the release of inflammatory cytokines such as IL-1β and IL-18 [15]. Nowadays, the role of pyroptosis in cancer is two-sided. Pyroptosis may promote tumor growth by providing an inflammatory microenvironment [16]. The expression of GSDMD (the classical executioner of pyroptosis) was positively correlated with tumor-node-metastasis staging in non-small cell lung cancer [17]. However, pyroptosis also inhibited tumor growth by triggering cell death, which was one principle for anti-tumor durg to work [18,19]. Ferroptosis, an iron-dependent form of non-apoptotic cell death serves a vital role in tumor suppression [20,21]. Several regulators, such as KRAS, TP53, NFE2L2, YAP, NFS1, STYK1, LSH, RNF113A, and non-coding RNA participate in lung cancer development via shaping ferroptosis sensitivity. Moreover, traditional chemotherapeutic drugs or immunotherapy combined with can synergistically inhibit tumor proliferation during lung cancer therapy [22].

However, the orchestrate subroutines of RCD have not explored comprehensively in lung adenocarcinoma. Hereto, we integrated collected the hub-genes of RCD subroutines and compressively analyzed these hub-genes synergistic effect in predicting LUAD prognosis and immunotherapy benefit.

2. Materials and methods

2.1. Raw data

The RNA sequence data (FPKM and Counts values) and clinical information in TCGA-LUAD cohort (59 normal tissue and 526 lung adenocarcinoma tumor tissue) were downloaded from the UCSC Xena database (http://xena.ucsc.edu/). GSE70294 containing gene expression arrays and survival data in 442 lung adenocarcinoma patients were picked out for the analysis. Missing survival time or less than 30 days were excluded from the analysis. Twelve regulated cell death (RCD) patterns (Pyroptosis, Parthanatos, Oxeiptosis, Netotic cell death, Necroptosis, Lysosome-dependent cell death, Ferroptosis, Entotic cell death, Cuproptosis, Autophagy, Apoptosis and Alkaliptosis) related genes were extracted from previous study [23] and FerrDb database (http://www.zhounan.org/ferrdb). Altogether, 1254 concatenated genes related to RCD were brought into the following analysis.

2.2. RCD genes expression and prognosis analysis in LUAD

The sample distribution pattern in TCGA-LUAD cohort was used the principal component analysis (PCA). $|\log FC| > 1$ and FDR value < 0.05as the cutoff point to recognize the differentially expressed RCD-related genes (DEGs) through R package “limma”, “deseq2” and “edgeR”. The heatmap and Venn diagram was applied to visualize the result. Univariate Cox regression and Kaplan-Meier (KM) analysis was used to determine the DEGs associated with patients’ overall survival (OS) time.

2.3. Unsupervised clustering

The univariate Cox algorithm was employed to screen out the RCD genes associated with overall survival time, and genes with p value < 0.05 were selected for non-negative matrix factorization (NMF) unsupervised clustering. We select values of k as the best rank value where the magnitude of the cophenetic correlation coefficient begins to fall.The Kaplan Meier method was used to estimate the difference in overall survival (OS) between different clusters.

2.4. Construction the RCD-related risk model

Removing the tumor samples with missing survival information, we constructed the risk model based on the data of 513 LUAD patients in TCGA cohort, and the data of GSE70294 as a validation cohort. Uni-cox and KM analysis using the survival R package to screen RCD genes associated with patients’ prognosis from TCGA and GSE70294 datasets with an inclusion criteria p value < 0.05. Then, the intersection genes from the above two datasets were analyzed by the LASSO regression to narrow the range of prognostic RCD genes. The Akaike information criterion (AIC) method of multivariate Cox regression analysis was applied to develop an optimal risk model based on the AIC value and concordance index. The risk score was calculated as follows:

$$\text{Risk score} = \sum_{i=1}^{N} (\text{coefi} \times \text{expi})$$

where coefi is multivariate Cox regression coefficient and expi is the expression of RCD genes. To investigate the independent prognostic factors for LUAD patients, univariate and multivariable Cox regression analyses were used.

2.5. Development and assessment the nomogram

Integrating all independent prognostic factors, the R package "RMS" was used to develop a nomogram model. Nomogram calculated the probability of clinical events via integrating scores for each influencing factor in the prediction model. Calibration curves and time ROC curves were leveraged to assess accuracy of the nomogram.

2.6. Functional annotation based on the risk model

Functional enrichment between high- and low-risk group according to the risk model was investigated using the "clusterProfiler", "pathview", "limma", "msigdbr" and "GSVA" packages. The "limma" package determined DEGs in different risk groups with a logFC of 1 and a p value of <0.05. p value was adjused by BH methods. Subsequently, the "clusterProfiler" and "pathview" package recognized the distinct GO biological processes and KEGG pathways enriched in the high-risk and low-risk groups based on DEGs set. The GSVA algorithm followed steps: "msigdbr" R package retrieved and download the GO and KEGG gene set from GSEA website (https://www.gsea-msigdb.org/). And then, "GSVA" packages calculated function annotation enrichment score for each sample. Finally, "limma" package compared the differentially expression pathway in different risk groups and select top 20 pathway to draw heat map.

2.7. Estimation of tumor immunity characteristics

The Cancer-Immunity cycle is a series of stepwise antitumor events, which initiated by oncogenesis [2]. The Cancer-Immunity Cycle can be divided into seven major steps, and each step requires the coordination of numerous factors, both stimulatory and inhibitory in nature. Dysfunction of inhibitory factors reduce immune activity and provide convenience for tumor escape. To screen potential immunosuppressive targets, the expressed levels of these inhibitory genes were explored on basis of RCD-risk signatures. These inhibitory genes were retrieved from TIP database (http://biocc.hrbmu.edu.cn/TIP/). The infraction of immune cell as a key step in Cancer-Immunity Cycle, single sample gene set enrichment analysis (ssGSEA) was adopted to quantify the enrichment level of immune cells in the tumor microenvironment.

2.8. Evaluation of tumor immunotherapy based on risk model

The association of immune checkpoint inhibitors (ICIs), including PCDD1, CTLA4, CD274, CD40, CD160, TNFSF15, LAG3, KIR3DL1, ADORA2A, TIGIT, and DCD1LG2, with the risk score were estimated by R package "corrplot". The benefit of ICIs was compared between high-risk and low-risk group on basis of The Cancer Immunome Database (TCIA) (https://tcia.at/home) and TIDE website (http://tide.dfci.harvard.edu/).

2.9. Cell culture and transfection

The human bronchial epithelial cell line 16HBE and Lung cancer cell lines, including NCI-H1975 and A549, were purchased from Cell Bank/Stem Cell Bank, Chinese Academy of Sciences (Shanghai, China) and were cultured in DMEM (Gibco, USA) supplemented with 10 % FBS (Gibco), and 1 % penicillin/streptomycin (Solarbio, China) at 37 °C in a humidified incubator with 5 % CO2. Small interfering RNAs (siRNAs) were obtained from RiboBio (Guangzhou, China) and transfection was performed using Lipofectamine 3000 (Invitrogen, USA) following the manufacturer's instructions.

2.10. RNA isolation and quantitative real-time PCR assay

Total RNA was isolated from cells with TRIzol reagent (Takara, Japan), and cDNA was generated using the PrimeScript™ RT kit (Takara). Real-time PCR was performed in TB Green Premix Ex Taq (TaKaRa) in accordance with the protocol. The relative expression levels of the target genes were determined by the $2-\Delta\Delta CT$ method, and GAPDH was employed as the internal control. The primer we use is as follows:

GAPDH: 5' - 3′ Forward: GGAGCGAGATCCCTCCAAAAT, Reverse: GGCTGTTGTCATACTTCTCATGG.

KRT8: 5' - 3′ Forward: TCCTCAGGCAGCTATATGAAGAG, Reverse: GGTTGGCAATATCCTCGTACTGT.

2.11. Western blot

Cells were lysed in RIPA lysis buffer (Beyotime Biotechnology, China) supplemented with PMSF (Solarbio, China). Proteins were resolved on SDS-PAGE gel and then transferred onto PVDF membranes (Millipore, USA). Subsequently, the transfer membrane was blocked with 5 % non-fat milk at room temperature, further incubated overnight at 4 °C with the specific primary antibodies (anti-KRT8 and anti-β-actin). The protein bands were displayed with enhanced ECL chemiluminescence detection reagent (Beyotime Biotechnology).

2.12. Cell migration and invasion assays

Cell migration and invasion assays were performed using 24-well transwell chambers (Corning, USA) with or without Matrigel.

After 48 h of incubation, cells in the upper chamber migrated or invaded the lower surface, which were fixed and stained. These cells were subsequently counted and compared. Wound healing assay was conducted to determine the ability of cells to migrate. The tip of a 10-μL pipette was used to create a gap, and serum-free medium was added to the cells for a further 48 h.

2.13. Colony formation assays

NCI-H1975 or A549 cells were inoculated into 6-well plates at 1×10^3 cells per well for 10 days. After fixing and staining, the number of clones was counted and analyzed by microscope.

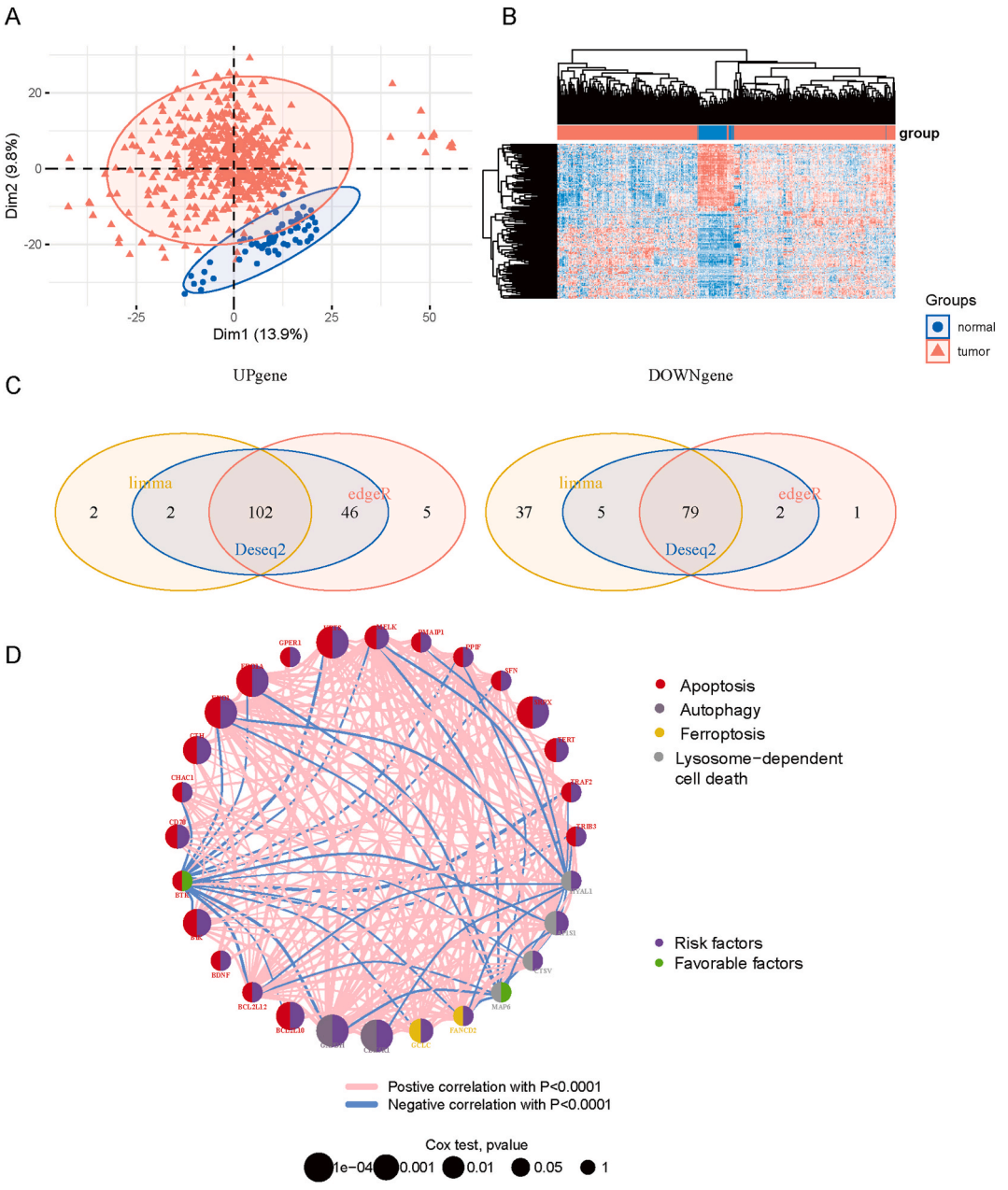

Fig. 1. Identification the DEGs and prognostic genes (a) PCA showed the sample distribution pattern in TCGA-LUAD (b) Heatmap (blue: low expression level; red: high expression level) of the RCD-related genes between the normal and tumor group (c) The intersected DEGs on basis of R package "Deseq", "limma", and "edegeR" (d) Interactions among 28 prognostic DEGs.

2.14. Statistical analysis

All data processing, statistical analysis, and plotting were performed using R software (version 4.2.3). Comparisons between groups were assessed using the Student's t-test and one-way ANOVA. GraphPad Prism 8.3.0 software was used to analyze the data and plot the diagrams. P value < 0.05 was considered statistically significant in all results.

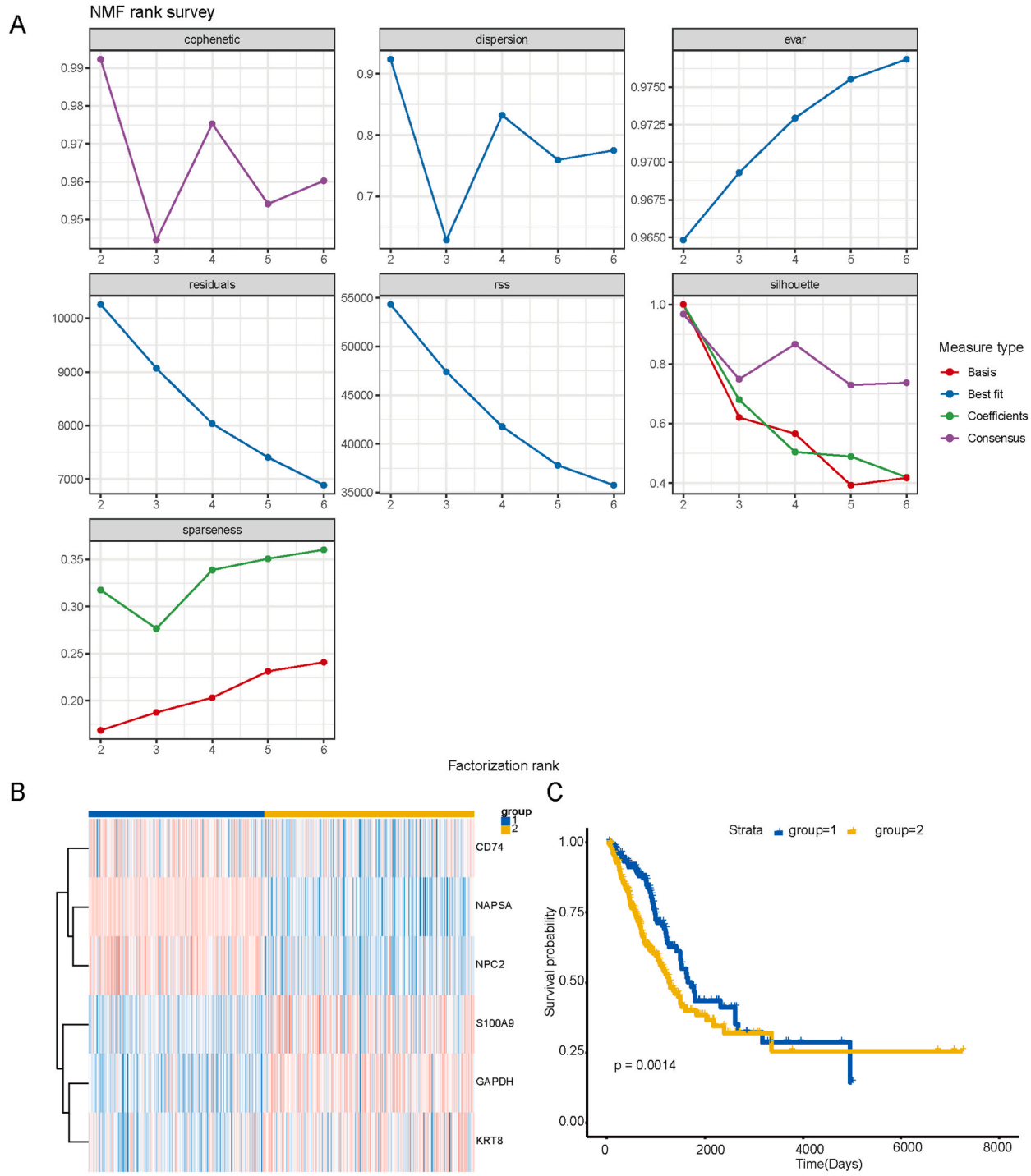

Fig. 2. Identification the molecular cluster based on the expression of RCD genes (a) Selection of optimal κvalue in NMF rank survey (b) 503 LUAD patients were divided into cluster 1 and cluster 2 according to the optimal $\kappa = 2$ (c) Heatmap (blue: low expression level; red: high expression level) of key NMF clustering signatures between the cluster1 and cluster 2 (d) The survival analysis between cluster 1 and cluster 2.

3. Results

3.1. Identification the DEGs and prognostic genes

The sample distribution pattern in TCGA-LUAD was shown in Fig. 1A. The heat map of the full range of RCD genes was shown in Fig. 1B. Using an p value < 0.05 and $|\log FC| > 1$ as the cutoff criteria, a total of 181 DEGs, including 102 upregulated genes and 79 downregulated genes, were picked out (Fig. 1C). The Kaplan Meier method and unicox identified 28 prognostic genes from the DEGs in p value < 0.05, and the interaction network in 28 genes was showed in Fig. 1D.

3.2. Identification the molecular cluster based on the expression of RCD genes

Using univariate Cox regression survival analysis with $P < 0.05$ as the cutoff criteria, a total of 208 RCD genes were performed the NMF clustering. The rank value was the optimal, when the cophenetic value was 2 (Fig. 2A). 503 LUAD patients were divided into cluster 1 and cluster 2 based on 6 key signatures (CD74, NAPSA, NPC2, S100A9, GAPDH, and KRT8) (Fig. 2B and C). The LUAD patients in cluster 2 had a worse prognosis compared with the patients in cluster1 (Fig. 2D).

3.3. Establishment risk model based on seven RCD-related gene signatures

1254 RCD genes were subjected to univariate Cox and K-M analysis in TCGA and GSE70294 datasets, and a total 57 genes were determined (Fig. 3A). Subsequently, 18 lasso genes with the best lambda value were screen out following LASSO analysis (Fig. 3B and

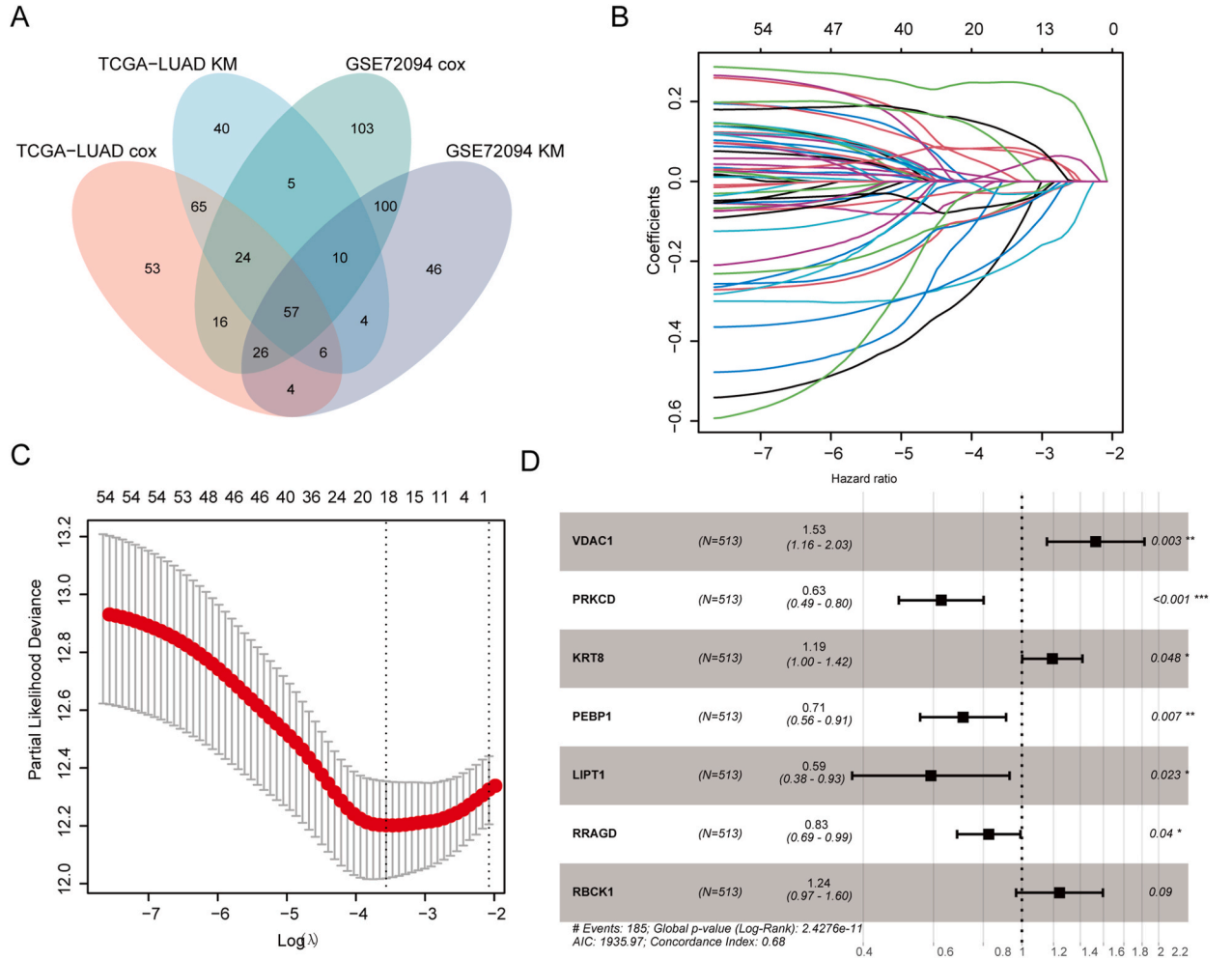

Fig. 3. Construction the optimal risk model (a) Intersecting genes associated with LUAD patients' overall survival in the TCGA and GSE70294 (b) LASSO coefficient profiles of the 57 prognostic RCD genes in the TCGA cohort (c) Selection of the optimal lambda (d) The AIC method of multivariate Cox regression analysis select 7 risk signatures to establish the optimal risk model.

C). To construct the optimal risk model, the AIC method of multivariate Cox regression analysis chose 7 genes returned from the 18 lasso genes (Fig. 3D). Among 7 genes, VDAC1, KRT8, and RBCK1 were risk factors for LUAD patients' OS, and PRKCD, PEBP1, LIPT1 and RRAGD were protective factors. A risk score was assigned to each LUAD patient according to the constructed prognostic model (Risk score = 0.4253* VDAC1 expression + −0.4659* PRKCD expression + 0.1753* KRT8 expression + −0.3397* PEBP1 expression + −0.5256* LIPT1 expression + −0.1914* RRAGD expression + 0.2166* RBCK1expression), and LUAD patients were categorized into high-risk and low-risk groups according the medium of risk score. The KM survival curve revealed that high-risk group in the TCGA cohort and GSE70294 cohort had poorer prognosis than the low-risk group. The AUC of time-dependent receiver operating characteristics curve predicted 1-, 3-, and 5 years OS. The corresponding AUC values in the TCGA cohort was 0.72, 0.70, and 0.67, respectively (Fig. 4C), while those in the GSE70294 cohort were 0.73, 0.74, and 0.72 (Fig. 4D).

3.4. Construction and evaluation of the nomogram

Based on the result of multivariate Cox analysis, nomogram was leveraged to accurately predict the overall survival rate for 1-, 3-, and 5-year (Fig. 5A) via quantifying the contributions of stage and risk score. The calibration curves constructed on basis of the TCGA cohort demonstrated that the predictive OS value and observed OS value were highly identical (Fig. 5B). Furthermore, the AUC for 1-, 3-, and 5-year were 0.756, 0.741 and 0.711, respectively (Fig. 5C). These results were consistent with those obtained GSE70294 cohort (Fig. 5D–F), implying that the constructed nomogram have a promising ability to predicting the overall survival rate for LUAD.

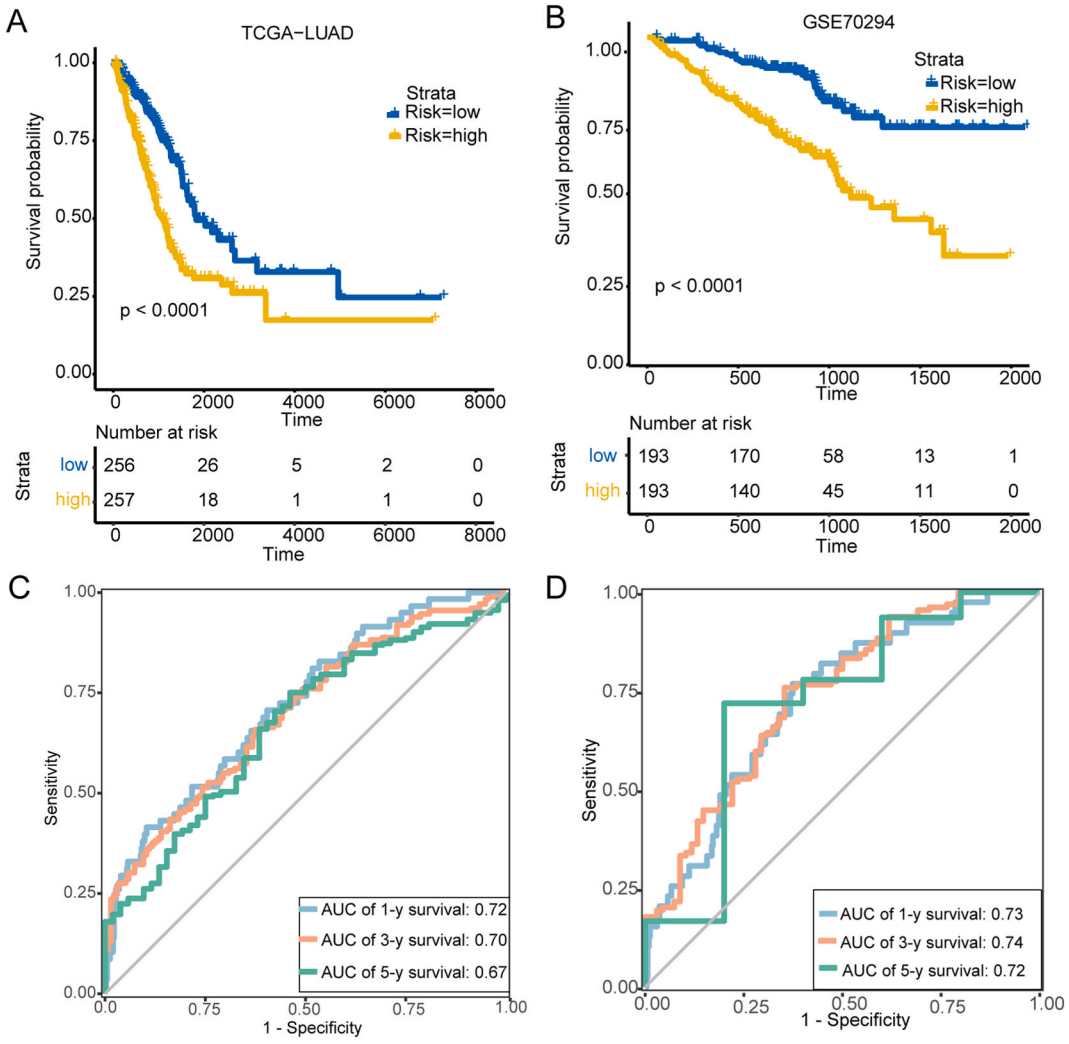

Fig. 4. The evaluation of risk model (a,b) The Kaplan-Meier survival curve with different risk groups in the (a)TCGA cohort and (b) GSE70294 (c, d) The ROC of risk model in the (c) TCGA cohort and (d) GSE70294 cohort.

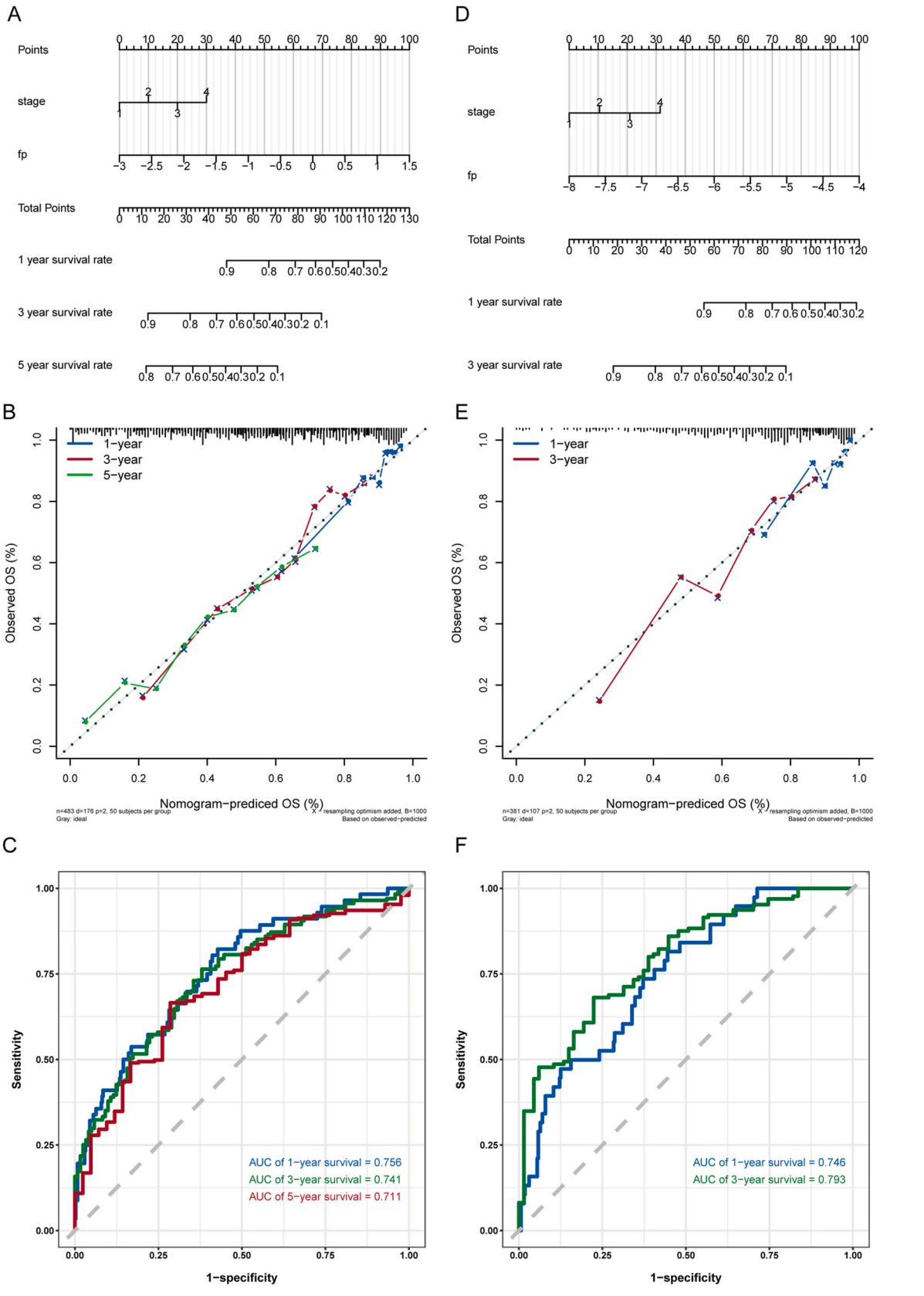

(caption on next page)

Fig. 5. Establishment and assessment the nomogram (a) Construction the nomogram based on the TCGA dataset (b) Calibration curve and (c) time ROC curve assessed the accuracy of TCGA-nomogram (d) Construction the nomogram based on the GSE70294 dataset (e) Calibration curve and (f) time ROC curve assessed the accuracy of GEO-nomogram.

3.5. Functional enrichment based on risk model

To explain differences in high- and low-risk group based on the risk mode, we utilized the GO and KEGG analysis based on the DEGs to investigate the potential molecular mechanism. The result of GO revealed that humoral response, platelet degranulation, collagen−containing extracellular matrix, platelet alpha granule and endopeptidase inhibitor activity were mainly enriched (Fig. 6A). Meanwhile, KEGG revealed that DEGs were mainly enriched in complement and coagulation cascades, Amoebiasis and alpha−Linolenic acid metabolism (Fig. 6B). The GSVA result revealed that folate biosynthesis pathway, pentose phosphate pathway, galactose metabolism pathway, p53 signaling pathway significantly enriched in high-risk group, while proteasome pathway and pathogenic Escherichia coli infection pathway significantly enriched in low-risk group (Fig. 6C).

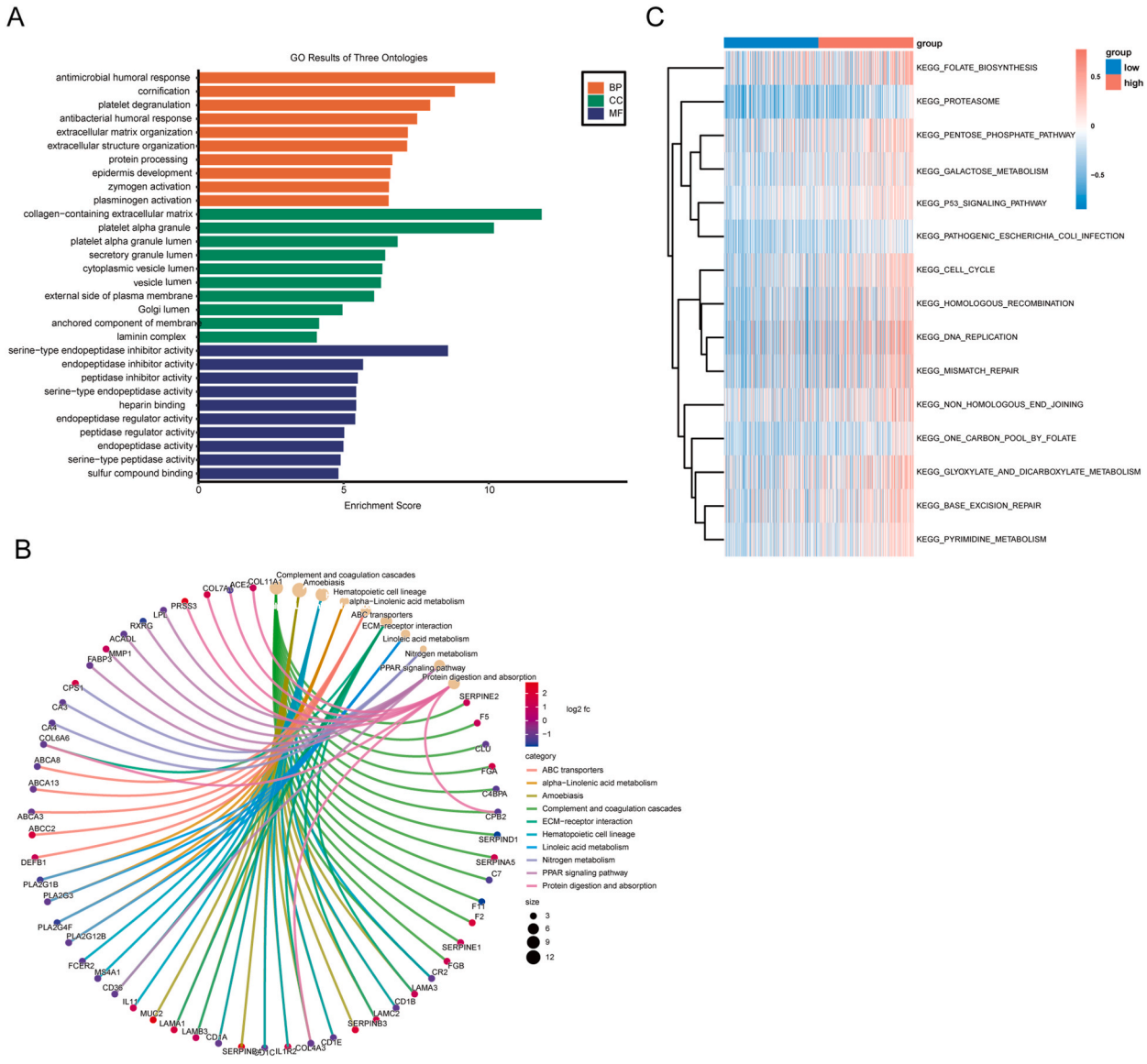

Fig. 6. Functional annotation based on risk model (a) GO term and (b) KEGG pathway enrichment according to the DEGs in different risk group (c) GSVA enrichment analysis.

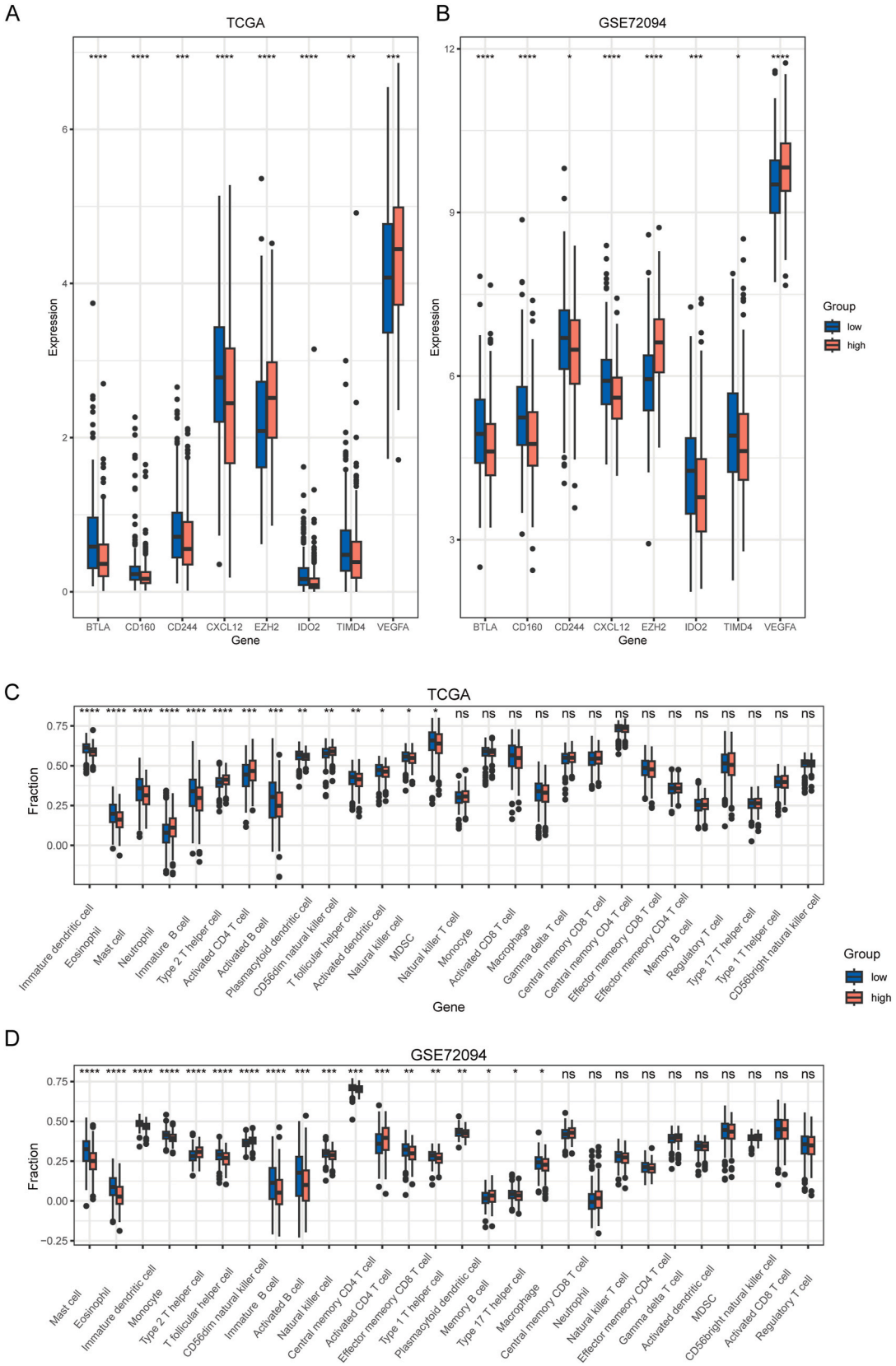

(caption on next page)

Fig. 7. The tumor immunity analysis. (A) The expression of Cancer-Immunity Cycle suppressor (BTLA, CD160, CD244, CXCL12, IDO2, TIMD4) in TCGA cohort and (B) GSE70294 cohort; (C) The fraction of tumor-infiltrating immune cells in TCGA cohort and (D) GSE70294 cohort.

3.6. Interaction of RCD risk signature and tumor immunity

The expression of Cancer-Immunity Cycle suppressor (BTLA, CD160, CD244, CXCL12, IDO2, TIMD4) in TCGA and GSE70294 cohorts were highly expressed in the low-risk group, while the expression of EZH2 and VEGFA were lowly expressed in high-risk group (Fig. 7A and B). Multiple immune cell such as immature dendritic cell, Eosinophil, Mast cell, immature B cell, Activated B cell,

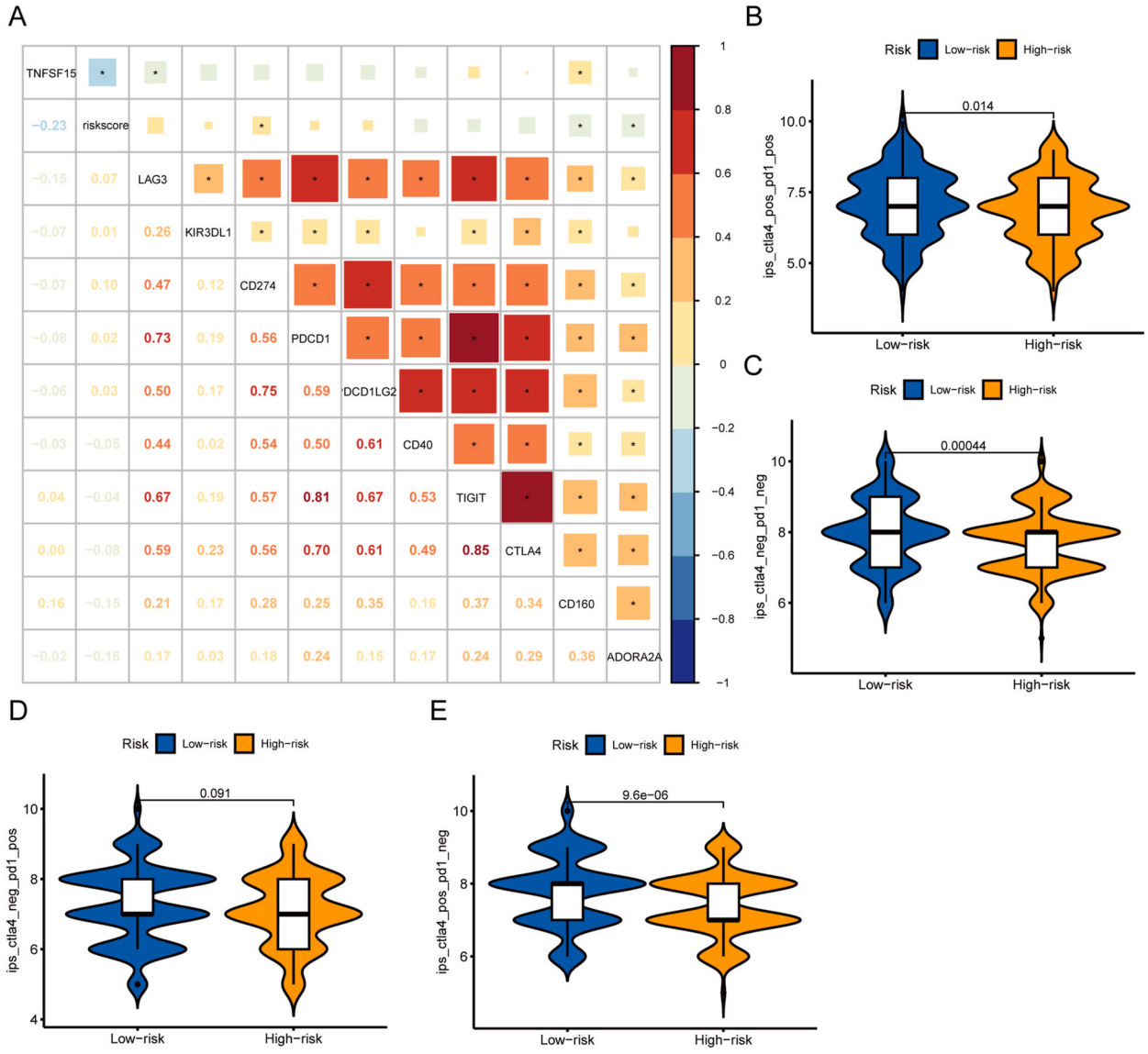

Fig. 8. The expression of ICs and IPS score analysis in risk model. (A) The relationship between risk score and ICIs expression; (B–E) Comparation IPS score in different risk groups.

As shown in Fig Figs. S1A–E, qRT-PCR and Western blot assays indicated that KRT8 expression was significantly higher in NCI-H1975 and A549 than that in normal human bronchial epithelial cells (16HBE). To investigate the biological function of KRT8 in lung cancer cells, si-KRT8# 1 and si-KRT8#2 was adopted to decrease the expression of KRT8. After transfection, KRT8 expression was significantly decreased to varying degree. Transwell assays (Figs. S2A–D) and the wound healing assay (Figs. S3A and B) showed that KRT8 knockdown markedly repressed the migration and invasion of NCI-H1975 and A549 cells. Furthermore, we found that colony formation ability was effectively inhibited when KRT8 was down-regulated in lung cancer cells (Figs. S4A and B). The expression of C-Myc, CDK4 and Cyclin D1/E1 in NCI-H1975 and A549 was measured by Western blot assay after KRT8 knockdown. The results revealed that C-Myc, CDK4 and Cyclin D1/E1 expressions were significantly decreased in the KRT8 knockdown group compared with the control group (Figs. S5A–C). It demonstrates that KRT8 is strongly associated with cell cycle process. Collectively, we conclude that KRT8 is involved in the regulation of lung cancer and contribute to lung cancer progression.

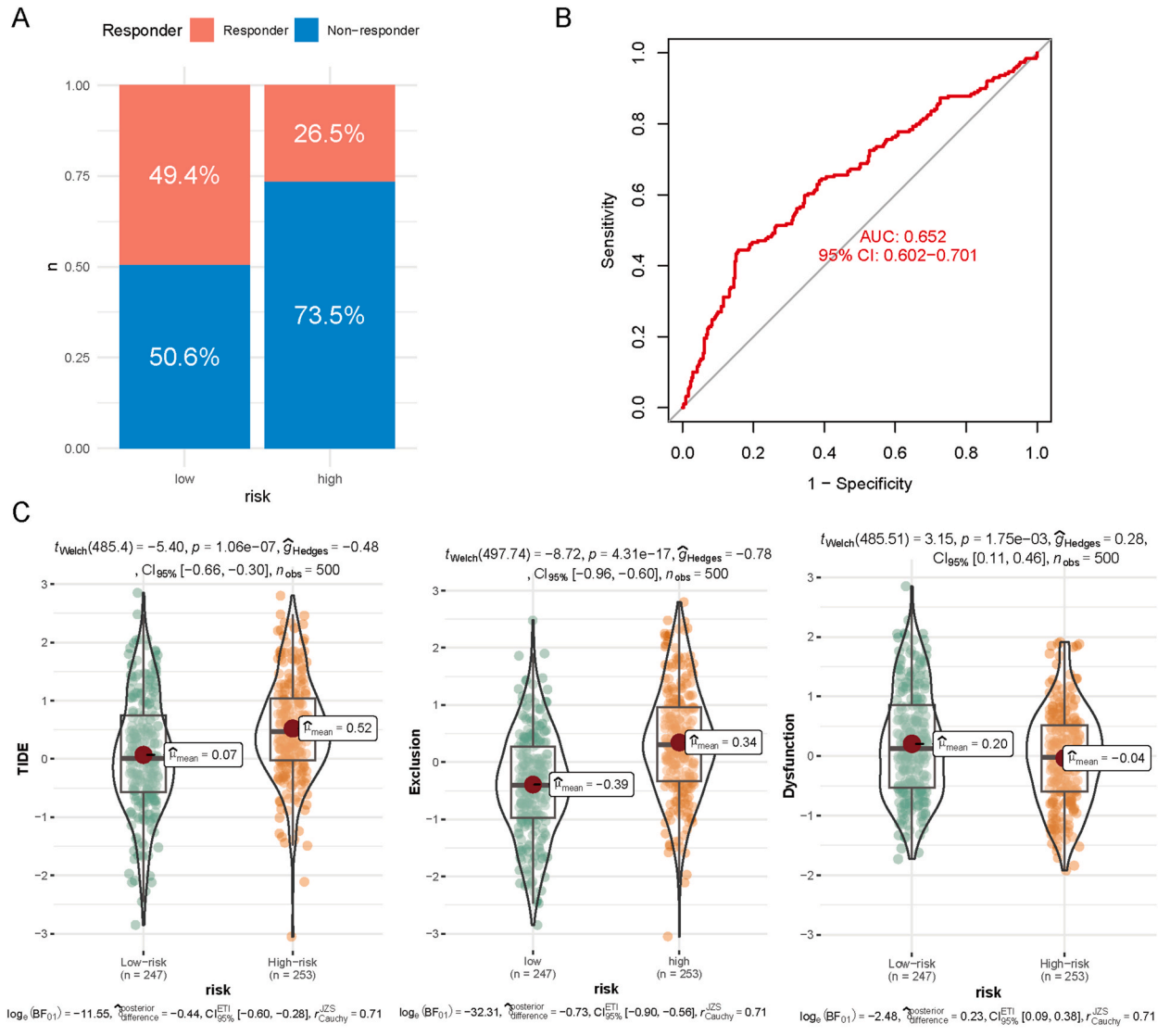

Fig. 9. Predicting immunotherapy response in different groups. (A) Comparing the responder ration in high-risk and low-risk groups; (B) ROC evaluated the accuracy of risk score in predicting immunotherapy response.

Plasmacytoid dendritic cell, Natural killer cell, T follicular helper cell, were also found to be enriched in the low-risk groups (Fig. 7C and D). In addition to Cancer-Immunity Cycle suppressor gene mentioned above, ICs also suppress the tumor immunity. Therefore, we also probe into the association between the expression of ICs and risk score and found the expression levels of ICs were negatively associated with risk score (Fig. 8A). Considering the vital roles played by ICs in tumor immunotherapy, we further compared the ICs response in the high- and low-risk groups via TCIA and TIDE databases. In the TCIA data, the low-risk group showed a better immunotherapeutic effect (Fig. 8B–E). Meanwhile, the patients with low risk had a higher responder ratio than those with high risk from the TIDE (Fig. 9A and B). Furthermore, the high-risk group exhibited a higher possibility of immune escape (Fig. 9B–D).

3.7. KRT8 exerts an oncogenic role in lung cancer

As shown in Figure S1 A-E, qRT-PCR and Western blot assays indicated that KRT8 expression was significantly higher in NCI-H1975 and A549 than that in normal human bronchial epithelial cells (16HBE). To investigate the biological function of KRT8 in lung cancer cells, si-KRT8# 1 and si-KRT8#2 was adopted to decrease the expression of KRT8. After transfection, KRT8 expression was significantly decreased to varying degrees. Transwell assays (Figs. S2A–D) and the wound healing assay (Figs. S3A and B) showed that KRT8 knockdown markedly repressed the migration and invasion of NCI-H1975 and A549 cells. Furthermore, we found that colony formation ability was effectively inhibited when KRT8 was downregulated in lung cancer cells (Figs. S4A and B). The expression of C-Myc, CDK4 and Cyclin D1/E1 in NCI-H1975 and A549 was measured by Western blot assay after KRT8 knockdown. The results revealed that

C-Myc, CDK4 and Cyclin D1/E1 expressions were significantly decreased in the KRT8 knockdown group compared with the control group (Figs. S5A–C). It demonstrates that KRT8 is strongly associated with cell cycle process. Collectively, we conclude that KRT8 is involved in the regulation of lung cancer and contribute to lung cancer progression.

4. Discussions

Lung cancer is the second frequently occurring cancer, and LUAD comprises around 40 % of all lung cancer. LUAD as one of the most aggressive and rapidly fatal tumor types, the overall survival of patients less than 5 years [24]. Moreover, patients with LUAD show high resistance to conventional radiotherapies and chemotherapies. Based on the current research results, the sensitivity of treatment and tumor progress were closely related to the susceptibility of LUAD tumor cells to undergo cell death [25]. Considering different RCD patterns showed a considerable degree of crosstalk, we collected the hub-genes of 12 RCD patterns and compressively analyzed these hub-genes synergistic effect in predicting LUAD prognosis and immunotherapy benefit.

In present research, we collected 1254 concatenated genes related to 12 RCD patterns. Survival analysis, LASSO and AIC of multivariate Cox regression analyses were performed successively, and we eventually determined 7 RCD-risk signatures (VDAC1, KRT8, RBCK1, PRKCD, PEBP1, LIPT1, and RRAGD) and established a risk model. The patients with high-risk exhibited poorly survival. And GSVA result also revealed that p53 signaling pathway significantly enriched in high-risk group. Of the 7 RCD-risk signatures, VDAC1, KRT8, and RBCK1 were risk factors for LUAD patients' OS, and PRKCD, PEBP1, LIPT1 and RRAGD were protective factors. VDAC1 is a key player in mitochondria-mediated apoptosis and ablation of VDAC1 inhibit multiple cancer cells including lung cancer cell proliferation, induce the modulation of tumor microenvironment components, and promote metabolic reprogramming and inflammation, which influences cancer progression, migration, and invasion [26–28]. LUAD patients with high KRT8 expression significantly reduced overall survival and recurrence-free survival [29]. PRKCD also known as PKCδ promotes non-small-cell lung cancer cell survival and chemotherapeutic resistance [30]. PEBP1 was a protective factor in LUAD, which was also confirmed by previous researches [31–33]. LIPT1 overexpression was associated with favorable outcome in breast cancer, clear cell renal cell carcinoma, ovarian cancer, and gastric cancer [34]. These previous researches were consistent with the result in present study.

KRT8 is a member of the keratin family. Previous research has shown that KRT8 is overexpressed in gastric cancer cells [35]. Wang et al. found that KRT8 is hypomethylated and highly expressed in lung adenocarcinoma, which is associated with poor prognosis [36]. In our study, we found that KRT8 promotes cell proliferation, migration and invasion of NCI-H1975 and A549 cells and linked to cell cycle progression.

Function annotation suggested that humoral response, platelet degranulation and complement, and coagulation cascades were significantly enriched, implying an interaction between RCD related-genes and the LUAD immune response. Furthermore, our research also explored the expression of Cancer-Immunity Cycle suppressor gene in different risk group. The high-risk group had a lowly expressed suppressor gene of tumor immunity. These finding were confirmed by previous researches in which RCD can alter tumor growth via modulating immune responses. In view of the treatment sensitivity may depend on the susceptibility of LUAD cell to undergo cell death. We further evaluated the risk model in predicting immunotherapy response and observed that the patients in low risk-risk group had a better response ratio. VDAC1 is involved in affecting inflammatory responses of macrophages, dendritic cells and $CD4^+$ T cells [37]. PRKCD promotes tumor progression by stimulating extracellular matrix (ECM) and PD-L1 expression which leads to immune exclusion and assists cancer cell escape from T cell surveillance in EGFR-mutated non–small cell lung cancer. Depletion of PRKCD enhances the T cell infiltration and significantly sensitizes the tumor to ICIs therapy (αPD-1) in vitro and in vivo [38].The role of other risk signatures in tumor immune has not been previously studied.

5. Conclusions

Collectively, the risk model based on 7 RCD-related risk signatures had a promising ability in predicting the OS of LUAD patients and facilitated the recognition of immunotherapy responder. The present study also had some limitations. The expression of prognostic 7 RCD-related risk signatures and the predictive value of the require additional evaluation on basis of the clinical case.

Funding

No funding.

Data availability statement

All data come from the publicly available datasets in present study. These datasets can be found here: TCGA database (http://cancergenome.nih.gov/), the GEO database (GSE70294) were included in this study, MSigDB datasets(http://www.gsea-msigdb.org/gsea/msigdb/index.jsp), TCIA website (https://tcia.at/home) and TIDE website (http://tide.dfci.harvard.edu/).

Conflict of Interest Disclosure Statement

The authors declare no potential conflicts of interest.

CRediT authorship contribution statement

Shan Gao: Writing – original draft, Validation, Supervision, Project administration, Methodology, Investigation. **Jiaqi Huang:** Writing – review & editing, Visualization, Supervision, Software, Methodology, Investigation, Formal analysis. **Rui Zhao:** Writing – review & editing, Validation, Supervision, Software, Project administration, Funding acquisition, Formal analysis, Conceptualization. **Haiqi He:** Writing – review & editing, Supervision, Resources, Project administration, Formal analysis, Data curation, Conceptualization. **Jia Zhang:** Writing – review & editing, Validation, Resources, Project administration, Methodology. **Xiaopeng Wen:** Writing – review & editing, Supervision, Software, Funding acquisition, Formal analysis, Data curation, Conceptualization.

Declaration of competing interest

The authors declare that they have no known competing financial interests or personal relationships that could have appeared to influence the work reported in this paper.

Acknowledgements

Not applicable.

Appendix A. Supplementary data

Supplementary data to this article can be found online at https://doi.org/10.1016/j.heliyon.2024.e38641.

References

[1] H. Sung, J. Ferlay, R.L. Siegel, M. Laversanne, I. Soerjomataram, A. Jemal, F. Bray, Global cancer statistics 2020: GLOBOCAN estimates of incidence and mortality worldwide for 36 cancers in 185 countries, CA Cancer J Clin 71 (3) (2021) 209–249.
[2] F. Nasim, B.F. Sabath, G.A. Eapen, Lung cancer, Med Clin North Am 103 (3) (2019) 463–473.
[3] F. Kocher, W. Hilbe, A. Seeber, A. Pircher, T. Schmid, R. Greil, J. Auberger, M. Nevinny-Stickel, W. Sterlacci, A. Tzankov, et al., Longitudinal analysis of 2293 NSCLC patients: a comprehensive study from the TYROL registry, Lung Cancer 87 (2) (2015) 193–200.
[4] U. Pastorino, M. Silva, S. Sestini, F. Sabia, M. Boeri, A. Cantarutti, N. Sverzellati, G. Sozzi, G. Corrao, A. Marchiano, Prolonged lung cancer screening reduced 10-year mortality in the MILD trial: new confirmation of lung cancer screening efficacy, Ann. Oncol. 30 (7) (2019) 1162–1169.
[5] N. Duma, R. Santana-Davila, J.R. Molina, Non-small cell lung cancer: epidemiology, screening, diagnosis, and treatment, Mayo Clin. Proc. 94 (8) (2019) 1623–1640.
[6] A.A. Thai, B.J. Solomon, L.V. Sequist, J.F. Gainor, R.S. Heist, Lung cancer, Lancet 398 (10299) (2021) 535–554.
[7] B. Melichar, Biomarkers in the management of lung cancer: changing the practice of thoracic oncology, Clin. Chem. Lab. Med. 61 (5) (2023) 906–920.
[8] L. Galluzzi, I. Vitale, S.A. Aaronson, J.M. Abrams, D. Adam, P. Agostinis, E.S. Alnemri, L. Altucci, I. Amelio, D.W. Andrews, et al., Molecular mechanisms of cell death: recommendations of the nomenclature committee on cell death 2018, Cell Death Differ. 25 (3) (2018) 486–541.
[9] M. Liao, R. Qin, W. Huang, H.P. Zhu, F. Peng, B. Han, B. Liu, Targeting regulated cell death (RCD) with small-molecule compounds in triple-negative breast cancer: a revisited perspective from molecular mechanisms to targeted therapies, J. Hematol. Oncol. 15 (1) (2022) 44.
[10] F. Peng, M. Liao, R. Qin, S. Zhu, C. Peng, L. Fu, Y. Chen, B. Han, Regulated cell death (RCD) in cancer: key pathways and targeted therapies, Signal Transduct Target Ther 7 (1) (2022) 286.
[11] R. Singh, A. Letai, K. Sarosiek, Regulation of apoptosis in health and disease: the balancing act of BCL-2 family proteins, Nat. Rev. Mol. Cell Biol. 20 (3) (2019) 175–193.
[12] B.A. Carneiro, W.S. El-Deiry, Targeting apoptosis in cancer therapy, Nat. Rev. Clin. Oncol. 17 (7) (2020) 395–417.
[13] S.T. Diepstraten, M.A. Anderson, P.E. Czabotar, G. Lessene, A. Strasser, G.L. Kelly, The manipulation of apoptosis for cancer therapy using BH3-mimetic drugs, Nat. Rev. Cancer 22 (1) (2022) 45–64.
[14] R.W. Johnstone, A.A. Ruefli, S.W. Lowe, Apoptosis: a link between cancer genetics and chemotherapy, Cell 108 (2) (2002) 153–164.
[15] J. Shi, W. Gao, F. Shao, Pyroptosis: gasdermin-mediated programmed necrotic cell death, Trends Biochem. Sci. 42 (4) (2017) 245–254.
[16] X. Xia, X. Wang, Z. Cheng, W. Qin, L. Lei, J. Jiang, J. Hu, The role of pyroptosis in cancer: pro-cancer or pro-"host"? Cell Death Dis. 10 (9) (2019) 650.
[17] J. Gao, X. Qiu, G. Xi, H. Liu, F. Zhang, T. Lv, Y. Song, Downregulation of GSDMD attenuates tumor proliferation via the intrinsic mitochondrial apoptotic pathway and inhibition of EGFR/Akt signaling and predicts a good prognosis in non-small cell lung cancer, Oncol. Rep. 40 (4) (2018) 1971–1984.
[18] Y. Feng, M. Li, X. Yangzhong, X. Zhang, A. Zu, Y. Hou, L. Li, S. Sun, Pyroptosis in inflammation-related respiratory disease, J. Physiol. Biochem. 78 (4) (2022) 721–737.
[19] R. Yuan, W. Zhao, Q.Q. Wang, J. He, S. Han, H. Gao, Y. Feng, S. Yang, B. Cucurbitacin, Inhibits non-small cell lung cancer in vivo and in vitro by triggering TLR4/NLRP3/GSDMD-dependent pyroptosis, Pharmacol. Res. 170 (2021) 105748.
[20] Y. Zhang, J. Shi, X. Liu, L. Feng, Z. Gong, P. Koppula, K. Sirohi, X. Li, Y. Wei, H. Lee, et al., BAP1 links metabolic regulation of ferroptosis to tumour suppression, Nat. Cell Biol. 20 (10) (2018) 1181–1192.
[21] M. Jennis, C.P. Kung, S. Basu, A. Budina-Kolomets, J.I. Leu, S. Khaku, J.P. Scott, K.Q. Cai, M.R. Campbell, D.K. Porter, et al., An African-specific polymorphism in the TP53 gene impairs p53 tumor suppressor function in a mouse model, Genes Dev. 30 (8) (2016) 918–930.
[22] S. Wu, C. Zhu, D. Tang, Q.P. Dou, J. Shen, X. Chen, The role of ferroptosis in lung cancer, Biomark. Res. 9 (1) (2021) 82.
[23] Y. Zou, J. Xie, S. Zheng, W. Liu, Y. Tang, W. Tian, X. Deng, L. Wu, Y. Zhang, C.W. Wong, et al., Leveraging diverse cell-death patterns to predict the prognosis and drug sensitivity of triple-negative breast cancer patients after surgery, Int. J. Surg. 107 (2022) 106936.
[24] T.V. Denisenko, I.N. Budkevich, B. Zhivotovsky, Cell death-based treatment of lung adenocarcinoma, Cell Death Dis. 9 (2) (2018) 117.
[25] K. Viktorsson, R. Lewensohn, B. Zhivotovsky, Systems biology approaches to develop innovative strategies for lung cancer therapy, Cell Death Dis. 5 (5) (2014) e1260.
[26] E. Zerbib, T. Arif, A. Shteinfer-Kuzmine, V. Chalifa-Caspi, V. Shoshan-Barmatz, VDAC1 silencing in cancer cells leads to metabolic reprogramming that modulates tumor microenvironment, Cancers 13 (11) (2021).
[27] T. Arif, L. Vasilkovsky, Y. Refaely, A. Konson, V. Shoshan-Barmatz, Silencing VDAC1 expression by siRNA inhibits cancer cell proliferation and tumor growth in vivo, Mol. Ther. Nucleic Acids 3 (4) (2014) e159.

[28] M.C. Brahimi-Horn, S. Giuliano, E. Saland, S. Lacas-Gervais, T. Sheiko, J. Pelletier, I. Bourget, F. Bost, C. Feral, E. Boulter, et al., Knockout of Vdac1 activates hypoxia-inducible factor through reactive oxygen species generation and induces tumor growth by promoting metabolic reprogramming and inflammation, Cancer Metab 3 (2015) 8.
[29] L. Xie, Y. Dang, J. Guo, X. Sun, T. Xie, L. Zhang, Z. Yan, H. Amin, X. Guo, High KRT8 expression independently predicts poor prognosis for lung adenocarcinoma patients, Genes 10 (1) (2019).
[30] A.S. Clark, K.A. West, P.M. Blumberg, P.A. Dennis, Altered protein kinase C (PKC) isoforms in non-small cell lung cancer cells: PKCdelta promotes cellular survival and chemotherapeutic resistance, Cancer Res. 63 (4) (2003) 780–786.
[31] A. Zhang, J. Yang, C. Ma, F. Li, H. Luo, Development and validation of a robust ferroptosis-related prognostic signature in lung adenocarcinoma, Front. Cell Dev. Biol. 9 (2021) 616271.
[32] Z. Ren, M. Hu, Z. Wang, J. Ge, X. Zhou, G. Zhang, H. Zheng, Ferroptosis-related genes in lung adenocarcinoma: prognostic signature and immune, drug resistance, mutation analysis, Front. Genet. 12 (2021) 672904.
[33] C. Ma, F. Li, H. Luo, Prognostic and immune implications of a novel ferroptosis-related ten-gene signature in lung adenocarcinoma, Ann. Transl. Med. 9 (13) (2021) 1058.
[34] Y. Liu, G. Luo, Y. Yan, J. Peng, A pan-cancer analysis of copper homeostasis-related gene lipoyltransferase 1: its potential biological functions and prognosis values, Front. Genet. 13 (2022) 1038174.
[35] J. Fang, H. Wang, Y. Liu, F. Ding, Y. Ni, S. Shao, High KRT8 expression promotes tumor progression and metastasis of gastric cancer, Cancer Sci. 108 (2) (2017) 178–186.
[36] W. Wang, J. He, H. Lu, Q. Kong, S. Lin, KRT8 and KRT19, associated with EMT, are hypomethylated and overexpressed in lung adenocarcinoma and link to unfavorable prognosis, Biosci. Rep. 40 (7) (2020).
[37] H. Hu, L. Guo, J. Overholser, X. Wang, Mitochondrial VDAC1: a potential therapeutic target of inflammation-related diseases and clinical opportunities, Cells 11 (19) (2022).
[38] Y.H. Zuo, W.N. Gao, Y.J. Xie, S.Y. Yang, J.T. Zhou, H.H. Liang, X.X. Fan, Tumor PKCdelta instigates immune exclusion in EGFR-mutated non-small cell lung cancer, BMC Med. 20 (1) (2022) 470.